e-Prime - Advances in Electrical Engineering, Electronics and Energy 9 (2024) 100721

Contents lists available at ScienceDirect

e-Prime - Advances in Electrical Engineering, Electronics and Energy

journal homepage: www.elsevier.com/locate/prime

Power converters design and experimental verification for electromagnetic contactors to reduce the impact of the voltage sag in the power system

Borislav Dimitrov [a,*], Khaled Hayatleh [b], Sylvia Konaklieva [a]

[a] *Warwick University, United Kingdom*
[b] *Oxford Brooks University, United Kingdom*

ARTICLE INFO

Keywords:
Electromagnetic contactor
Voltage sag
Totem-Pole PFC converter

ABSTRACT

This research aims to offer a power supply system based on power converters to supply electromagnetic contactors from the power distribution grid. Its primary purpose is to minimise the voltage sag impact on the contactor, eliminating the possibility of contacts tripping or excessive vibration. In addition to this, the contactor's inherent low power factor must be compensated, reducing the contactor's impact on the power grid. To complete these requirements, the power supply system comprises a Totem-pole PFC converter, a Buck converter stabilising the supplied voltage, and an H-Bridge, decreasing the switch-off commutation time. The research focuses on the converters' design methodology, supported by a case study and experimental verification. Considering the electromagnetic contactor characteristics, the system design requirements are systemised. The analytically and experimentally obtained data shows that based on the chosen converters' topologies, the suggested power supply system provides contactor stable operation in a wide input voltage range, acceptable power losses and high efficiency.

1. Introduction

The electromagnetic contactors, offered by many leading manufacturers [1-5], are an essential piece of equipment with many industrial applications. The main parts of a contactor are the electromagnetic system, AC or DC supplied, the contact system comprised of mechanical contacts and the arc extinguishing system. Although a well-known technology that has been around for decades, electromagnetic contractors are still an object of significant research. In [6], a novel construction specialised for switching between two power sources has been investigated. The dynamic characteristics of different novel electromagnetic systems have been objects of significant study [7,8,9], showing the modelling approaches based on equivalent circuits and Finite Element Analysis (FEA).

Recent investigation has also focused on classical plunger-type electromagnets, leading to their optimisation. For example, in [10] and [11], the application of FEA based on specialised software products is depicted, and the optimisation procedures are described. An electromagnetic system for specific operations has been demonstrated in [12], showing a DC electromagnet with an installed power of 22 kW.

The vibration of the AC electromagnetic system is one of the leading design components that determines its overall characteristics, reliability, and quality, as has been shown in [13]. The techniques for vibration mitigation have been an object of careful studies [14,15], including those specialised for aircraft and aerospace applications [16,17]. The precise analysis shows that the contact bouncing can be mitigated with specialised power supplies applied to the DC and AC electromagnets, as suggested in [18,19]. Based on different methods for contact vibration and bouncing experimental testing and measurement [20,21], their erosion due to the power supply influence can be registered and estimated precisely.

Another natural phenomenon occurring in the AC and DC contact apparatus is the electric arcing and sparking, which occurs between the contacts during their commutation [22-26]. Both phenomena have a negative effect on electric contacts, reducing their lifespan and determining the device's overall reliability. As research presents, the electric arc or spark can be turned on due to contact vibration provoked by electromagnetic power instability. Hence, AC or DC electromagnet voltage variation could increase electric contact erosion or provoke contact welding.

To solve the above-described problems, power converters with different topologies to supply the electromagnetic systems have been

* Corresponding author.
E-mail address: Borislav.Dimitrov@warwick.ac.uk (B. Dimitrov).

https://doi.org/10.1016/j.prime.2024.100721
Received 24 February 2024; Received in revised form 11 June 2024; Accepted 2 August 2024
Available online 17 August 2024

investigated. In [27], a technique for the switch-off time of an electric contactor's electromagnetic system is presented. A digitally controlled DC-DC converter used as a contactor's electromagnet power supply has been found in [28]. The system's primary purpose is to measure the coil impedance through the excitation voltage, coil current, and Pulse-Width-Modulation (PWM) duty cycle. The research shows that with 40 kHz PWM, the energy consumption during the contactors ON-state can be reduced. Another solution based on converters supply has been proposed in [29].

The above-presented advantages make the electronic power converter widely used for electromagnets [30-32]. In [30], a full bridge topology is applied to an electromagnet, operating with a closed-loop control with a current sense resistor integrated into the middle of the electromagnet's coil. Another study utilising a resonant converter as a contactor power supply system [31] shows the ability of a soft-switching technique to be achieved, increasing the average contact closing speed and reducing the contact closing time. Dedicated to the same aim, the research published in [32] shows the near-to-zero switching technique developed by a microprocessor system and a coil driver.

Another problem solved by power converters implemented as a part of the electromagnetic contactors and relays is the voltage sag and swell appearing in the power distribution system. The voltage sag manifests itself by a voltage drop with different durations, which can cause electromagnetic contactors to unintended tripping or permanent shutdown. The voltage swell is a sudden increase of the supplied AC voltage, generally detrimental for the electric/electronic equipment. Different methods for voltage sag measurement, estimation, and experimental study of its impact are developed. In [33], an evaluation method estimates random voltage sag waveforms and the AC contactors' operation under arbitrary sags.

To minimise the impact on the AC contactors and relays, various solutions accommodating electronic power supplies have been suggested [34,35]. In [36,37], voltage sag protection by switching between the main AC and auxiliary power supply has been studied. Power converters could also be used for voltage sag compensation, as shown in [38, 39]. An application of a dynamic voltage restorer based on bi-directional AC/AC converters to compensate for the voltage sag and swells has been presented in [38]. The experimental verification is done with a 2kVA prototype showing up to 94% peak efficiency and voltage sag/swell compensation, 25% and 50%, respectively. In [39], a contactor's power is completed by supplying an AC-DC rectifier, a DC-DC Boost converter with Power Factor Correction (PFC) and a two-switch DC-DC converter has been designed and experimentally tested. A case study has supported the converters' design procedures. The experimental setup shows 37% compensation of the voltage sag while keeping the power factor close to 0.97–0.98.

A future of the AC electromagnetic contactors is their low power factor due to the significant inductance of the electromagnet's bobbin. This requires a converter for Power Factor Correction (PFC) to be utilised as a part of the contractor's power supply system. The PFC converters are reviewed in [40], showing the main topologies. One of the advanced topologies is the Totem-pole PFC converter completed with GaN or SiC MOSFETs [41,42,43]. As shown in [44,45], this converter offers high efficiency and power density due to the reduced number of switches, zero crossing modulation and low power losses.

From the conducted literature review, the following conclusions are summarised:

- The contactors for industrial purposes are vulnerable to voltage sags in the power system, leading to contact tripping and major malfunctions or system blackouts. This problem can be solved using power converters to supply the contactor's electromagnetic system. Although different topologies have been studied [27-32], research on the overall system's efficiency improvement is necessary.
- The impact of power converters on the contactors' commutation phenomena, such as contact vibration, tripping, and commutation time, needs additional investigation. The electromagnetic system impact on the power switches manifested as overvoltage must be determined and accommodated as a part of the designed procedures. Also, recommendations for safety design margins, giving robust design, must be systemised.

This research aims to design a complete power supply system based on power converters to reduce the voltage sag impact on the electromagnetic contactors, ensuring their stable operation without contact tripping or vibrations. The power supply system must compensate for the electromagnetic system power factor, minimising its impact on the power distribution grid. As a result of the conducted research, requirements for the converter design must be concluded, giving high efficiency, power density and stable operation of the electromagnetic system considering its specific characteristics. Therefore, the novelty of this research consists of finding a unique solution based on a combination of well-known converter topologies, which ensures a match between the power distribution grid and the electromagnetic contactors at various conditions.

The rest of the paper is structured as follows: part 2 offers an analysis of the chosen power converter topologies and their operation supplying the electromagnetic system; part 3 presents a case study of the design procedure of the entire power supply system depicting the application of the fundamental theory; part 4 shows the experimental setup of the designed converters; part 5 offers a conclusion summarising the obtained results from design and experimental verification.

2. Analysis of the power converters for electromagnetic contactors

Table 1 shows systemised data of the contemporary three-phase electromagnetic contactors available on the market in the power range between 10 kW and 700 kW. The data collected from leading companies' catalogues [1-5] shows that the electromagnetic system's coil power varies between 100 W and 1300 W. The same data is depicted graphically in Fig. 1, showing the dependency between the conducted to the load power versus the coil power. The increased coil's power demand is proportional to the load power due to the increased size of the contact system and contact force.

A set of power converters is suggested to avoid the mutual impact between the electromagnetic contactor and the power system. The proposed topology is shown in Fig. 2. The converters' application and their choice justification could be arranged as follows:

Table 1
Estimated electromagnetic system coils' power.

Contactor coil power (W)	Maximum conducted power (kW)	Estimated conducted power to the three-phase load at different voltages (kW).		
		V minimum – V nominal – V maximum		
		180 V – 220 V – 240V	400 V – 440 V – 480V	500 V – 550 V – 600V
100	10	7.8	8.7	10.5
200	30	22.8	25.2	30.4
300	50	37.8	41.9	50.5
400	65	48.7	53.9	65
500	100	69.3	76.7	92.5
600	180	129.3	143.2	172.5
700	200	150	166	200
800	230	172.5	190.9	230
900	420	315	348.6	420
1000	500	375	415	500
1300	700	525	581	700

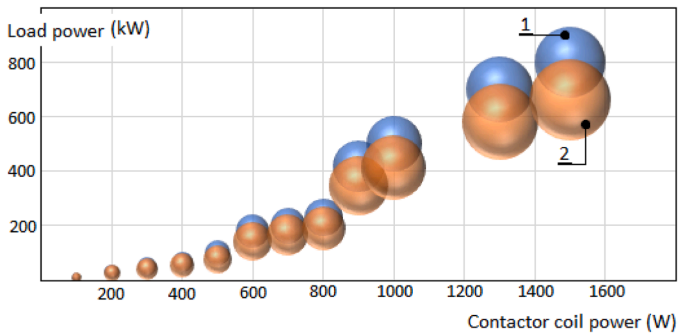

Fig. 1. Conducted power vs coil power of electromagnetic contactors. 1. Maximum conducted power; 2. Estimated power at different load voltages (Table 1).

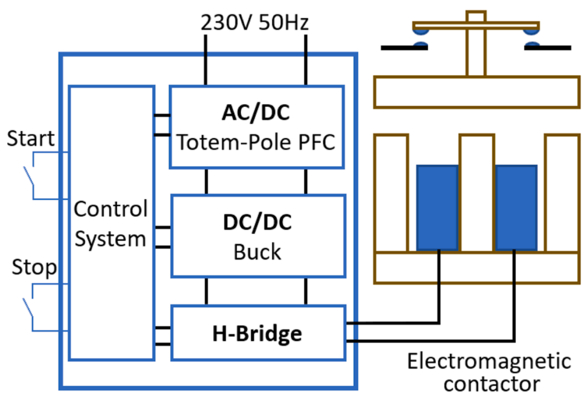

Fig. 2. Power converters with an electromagnetic contactor.

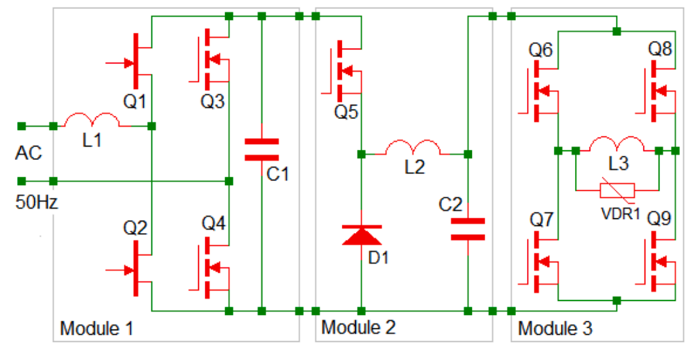

Fig. 3. Power converters for an electromagnetic contactor. Module 1 – Totem-pole PFC; Module 2 – Buck converter; Module 3 – H-bridge.

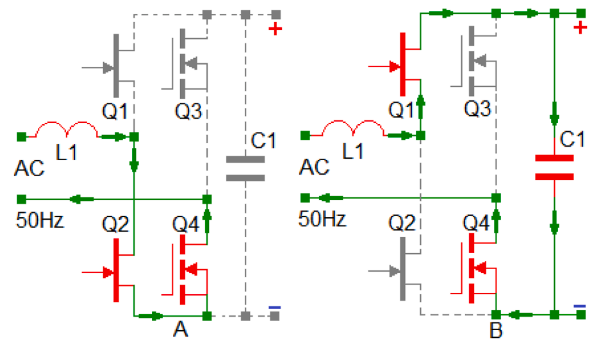

Fig. 4. Totem-Pole PFC converter. Positive half-period cycle. A) Transistor Q2 charges the inductor L1 through Q4; B) Transistor Q1 conducts the current through the output capacitor and the load through Q4.

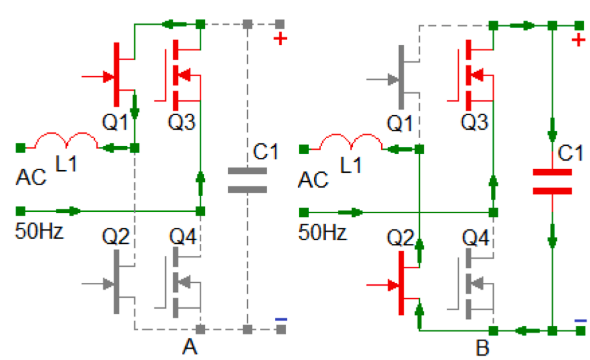

Fig. 5. Totem-Pole PFC converter. Negative half-period cycle. A) Transistor Q1 charges the inductor L1 through Q3; B) Transistor Q2 conducts the current through the output capacitor and the load through Q3.

- AC-DC Totem-pole PFC converter. As clarified from the researched literature [40-45], the Totem-pole topology has advanced characteristics that offer high power density and efficiency. In this topology, the main requirements for this converter are power factor compensation and operating in a wide input voltage range, compensating the system voltage sag.
- DC-DC buck converter. This converter is required to reduce the voltage after the Totem-pole converter, according to the electromagnetic system's voltage. The DC voltage could be applied to DC electromagnetic systems at the nominal rated voltage or to AC systems, recalculated and reduced to the required level to prevent coil damage. This requires a precise analysis of the AC and DC electromagnetic systems, which are experimentally estimated in this research. The buck converter was chosen for its main advantages: transformer-less topology, simplified structure and control technique, good efficiency, and power density.
- H-Bridge supplies the switch-on and switch-off processes to reduce the switch-off time.

The control system (outside the scope of this research) controls the converters and provides the interface with two start/stop buttons.

Fig 3 shows the power converter circuit elements according to the block diagram in Fig. 2. Module 1, the Totem-pole PFC, consists of two GaN transistors (Q1, Q2) for High-Frequency side (HF-side) switching, two MOSFET (Q3, Q4) for Low-Frequency side (LF-side) switching, input inductor L1 and filter capacitor C1. Module 2 is the Buck converter comprising transistor Q5, diode D1, inductor L2, and filter capacitor C2. The H-bridge is given in Module 3. It consists of four MOSFETs (Q6-Q9), supplying the contactor coil's L3.

During the positive half-period, Fig. 4, Q2 operates as a boost switch with duty cycle D, and Q1 operates with a D-1 duty cycle. The transistor Q4 is switched ON during the entire half period. Transistor Q3 is permanently switched off. Conversely, during the negative half-period, Fig. 5, Q1 operates as a boost switch with duty cycle D, and Q2 operates with a D-1 duty cycle. The transistor Q3 is switched ON during the entire half period, and Q4 is permanently switched off.

The Buck converter operation modes are shown in Fig. 6. This converter is controlled independently from the PFC converter. The transistor Q5 operates with duty cycle D, and the diode D1 operates with D-1.

The H-bridge modes of operation are depicted in Fig. 7. In the ON state (Fig. 7A), the contactor is supplied from the converters through transistors Q8 and Q7. The off-state (Fig. 7B) is supported with Q6 and Q9 to reverse the voltage over the coil, reducing the switching-off time. For this purpose, a short impulse with a duration equal to the contactor off-time and opposite polarity must be applied. A Voltage-dependent Resistor (VDR) is connected in parallel to L3 to reduce the commutation overvoltage.

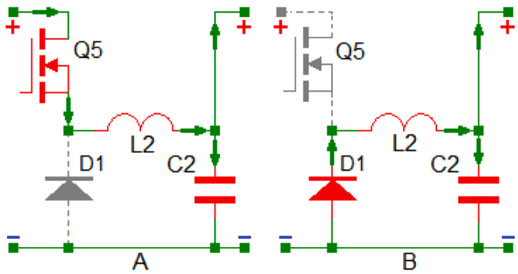

Fig. 6. Buck converter operation modes. A) Transistor Q5 (PWM controlled) is ON with duty cycle D; B) Freewheeling cycle through the diode D1 with duty cycle D-1.

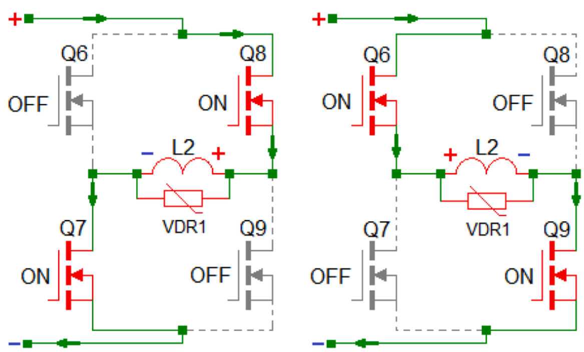

Fig. 7. Modes of operation of the H-Bridge. A) Contactor ON state; B) Contactor OFF state.

3. Design of the power converters

The design of the power converters follows a step-by-step analytical procedure, determining the main parameters of the power semiconductors and passive elements. The results are used for the parts selection. The design procedures are supported with a case study depicting their application in the practical design.

3.1. Design methodology of the power converters

The main equations for the power circuit design of the Totem-pole PFC converter are given in Table A.1 (Appendix) [40-45]. The design methodology starts with the input inductor calculation, including its inductance L_1, the maximum I_{Lmax} and RMS I_{Lrms} currents. The total inductor power loss $P_{L.total}$ is a sum of the conducted loss P_{Lcond} and the core loss P_{Lcore}, estimated according to the manufacturers' guidance [46, 47].

The High-Frequency side GaN transistors Q1 and Q2 are selected according to the results of the switching I_{sw} current and estimated input voltage. The total power loss $P_{Total.sw}$ is a sum of the conducting $P_{cond.sw}$ and switching $P_{switch.sw}$ for the transistor operating as a Boost switch. For the transistor operating as a rectifier, only the conducting $P_{cond.R}$ loss apply, calculated from the current $I_{Boost.R}$ through it.

The power loss $P_{MOSFET.R}$ for the Low-Frequency side, MOSFETs Q3 and Q4 can be estimated only based on the conductive power loss. The output capacitor C1 depends on the output power P_o, the output voltage range and the hold-up time t_{hold}. Capacitor's Equivalent Series Resistance (ESR) is determined based on the tanδ angle loss. H-Bridge transistors will dissipate only conductive loss, applied from two transistors connected in series. Eventually, the overall efficiency will be estimated based on the power loss of the three modules.

The Buck converter methodology is presented in Table A.2 (Appendix).

3.2. Case study

The case study aims to support the investigated converters' design procedure, given in Tables A.1 and A.2. Table 2 shows the input design parameters of the power part of the Totem-pole PFC, Buck and H-bridge modules, as shown in Fig. 3. The main requirements of the design system are as follows: a) to provide a stable operation in a wide input voltage range 90 – 265 $V\ AC$ compensating the voltage sag; b) operating with efficiency over 95% at a nominal voltage of 230 V AC; c) reducing the electromagnetic system coil current ripple to 2% at nominal conditions to ensure the stable operation of the contact system.

Table 3 shows the results obtained from the equations (1–33) applied to the input design parameters in Table 2. The data shows that an overall efficiency of 95% is achievable by following several design recommendations: a) The high-frequency side Totem-pole transistors must be enhancement mode GaN High-Electron-Mobility Transistors (HEMT) with no reverse recovery charge. Therefore, cascode GaN transistors are not acceptable for this design; b) Trade-off decision between minimising the inductor resistance, giving low power loss, and minimising its size, offering better power density, must be made; c) the MOSFETs could be 2 to 3 times oversized on Drain-Source current to minimise the conducting loss as a central part of the power loss in the LF Totem-pole PFC converter.

4. Experimental setup

The results of the experimental verification of the suggested system are depicted in Fig. 8–Fig. 17.

Fig. 8 shows the AC contactor direct supply from the power grid with nominal voltage 230 V, 50 Hz. The experimental circuits are supplied by a steady-state microgrid, which determines the input voltage shape and variable characteristics. Fig. 8A shows the experimental circuit with the allocation of current and voltage probes. It consists of a Solid State Relay (SSR) as a control switch to avoid the vibration of a contact switch and an oscilloscope. The laboratory equipment used (Fig. 8–Fig. 16) is as follows: AC mains 230 V; OSC – oscilloscope Keysight DSOX1204G; DC

Table 2
Input design parameters of the power supply system according to Fig. 3.

Parameter	Value	Parameter	Value
Totem-pole PFC converter (Module 1)		Buck converter (Module 2)	
Input voltage range	90 – 265 $V\ AC$; 50Hz	Input voltage maximum	450 $V\ DC$
Output voltage minimum	350 $V\ DC$	Input voltage minimum	320 $V\ DC$
Output voltage maximum	400 $V\ DC$	Output voltage minimum	180$V\ DC$
		Output voltage minimum	240$V\ DC$
Nominal power	500 W	Nominal power	500 W
Switching frequency	70 kHz	Switching frequency	100kHz
Inductor current ripple	20%	Inductor current ripple	2%
Hold-up time	10 ms		
Targeted PFC efficiency	98%	Targeted Buck efficiency	97%

H-Bridge (Module 3)	
Parameter	Value
Input—Output voltage (the transistors voltage drop is neglected)	180 V – 240V
Nominal power	500W
Targeted H-Bridge efficiency	99%
Targeted system efficiency	95%

Table 3
Design results according to the input parameters in Fig. 4.

Design parameters Totem-Pole PFC converter	Result	Equation
Inductor L_1, (Wurth, Iron powder toroid) Rdc	$220\mu H$; $45m\Omega$	(1)
Inductor L_1 losses and peak current	$1.54W$; $5.56A$	(2, 3, 4, 5)
HF side GAN transistors (IGLD60R190D1S) RMS current	$1.2A$	(6)
Switching and conducting and total GAN transistor power loss	$1W$; $0.9W$; $2.2W$	(7, 9, 10)
Total HF side power loss	$2.2W$	(13)
LF side MOSFET (IPA65R190C7XKSA1) RMS current	$1.33A$	(14)
Transistors power loss	$0.89W$	(15)
Totem-Pole PFC estimated efficiency η	98.8%	(33)
Output capacitor C_1; V_{Cmax}; R_{ESR}	$470\mu F$; $400V$; $20m\Omega$	(16, 17)
Output capacitor RMS current and power loss	$1.1A$; $24mW$	(18)
Buck converter		
Inductor L_1, (Wurth, Iron powder toroid) Rdc	$150\mu H$; $55m\Omega$	(21)
Inductor L_1 power loss and RMS current	$3.5W$; $5.56A$	(22, 23)
Transistor Q5 (IPA65R190C7XKSA1) total power loss	$5.77W$	(24, 25, 26)
Diode D_1 (RHRP1560) total power loss	$3.42\ W$	(27, 28)
Buck converter estimated efficiency η	97.2%	(33)
Output capacitor C_2; V_{Cmax}; R_{ESR}	$10\mu F$; $400V$; $20m\Omega$	(29, 30)
H-bridge		
Transistors $Q6 - Q9$ (IPA65R190C7XKSA1) power loss per transistor	$1.55\ W$	(31)
H-bridge total power loss with two ON series transistors	$3.1\ W$	(32)
H-bridge estimated efficiency	99.4%	(33)
Total estimated efficiency	95.3%	(33)

RS power supply 30 V 10A; Power analyser HMC8015 Rohde & Schwarz; SSR – Fotek 24–380 V.

Fig. 8B shows the voltage (1) and the current (2) at steady-state operation, giving a power factor of 0.56 and determining the suggested necessity of an active PFC correction electronics system. The transient turn-on process (Fig. 8C) depicts the peak current exceeding the 5–8 times nominal current.

Fig. 9 investigates the main AC contactor's times of turn-on (T1 = 16.35 ms, Fig. 9B), contact vibration (T2 = 3.41 ms, Fig. 9B) and turn-off (T3 = 8.45 ms, Fig. 9C). The experimental circuit (Fig. 9A) includes a current probe to measure the current (1) through the contactor's Normal Open (N.O.) contacts.

Fig. 10 shows a DC electromagnetic system powered from a DC source with a nominal voltage of 180 V (Table 2). Fig. 10A gives a turn-on time of T1=36.5 ms, measured between the contactor's DC voltage (1) and the current through the contactor's contacts. The turn-off time is T2=13.1 ms (Fig. 10B). The figure shows the coil voltage peak in the opposite direction (1) at the turn-off moment, which reaches several kilovolts without the VDR. The same experiment with the VDR (Fig. 10C) shows the voltage limitation to the VDR nominal voltage and current through the VDR of 1.06A with a continuation of 450µs.

Fig. 11 shows the experimental verification of the PFC Totem-pole converter, conducted separately with a variable resistor as a load (Fig. 11A). The input voltage (1) and current (2) waveforms with no PFC correction in stand-by operation are given in Fig. 11B. In this operation the power factor is 0.37. The power factor is corrected to 0.98 with a nominal power of 500 W (Fig. 11C).

Fig. 12 shows the experimentally verified efficiency of the Totem-Pole PFC converter, conducted with a power analyser (Fig. 12A). The maximum efficiency is 98.7% (Fig. 12B), which corresponds to the targeted efficiency in the design procedure (Table 4).

The voltage sag in the power line is depicted in Fig. 13. For experimental purposes, the waveform is obtained from a programable power supply.

Fig. 14 shows the effect of the voltage sag on the AC contactor directly powered by the power grid, as presented in Fig. 8 and Fig. 9. Contacts tripping (Fig. 14A) is registered with the voltage change over

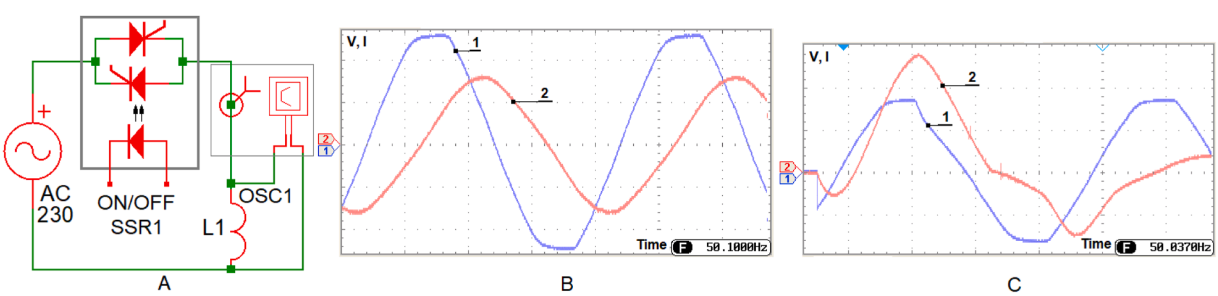

Fig. 8. Experimental verification of AC electromagnetic contactor. A – experimental circuit; B – sinusoidal voltage (1) and current (2) at steady-state conditions; C – voltage (1) and peak current (2) at turn-on transient process.

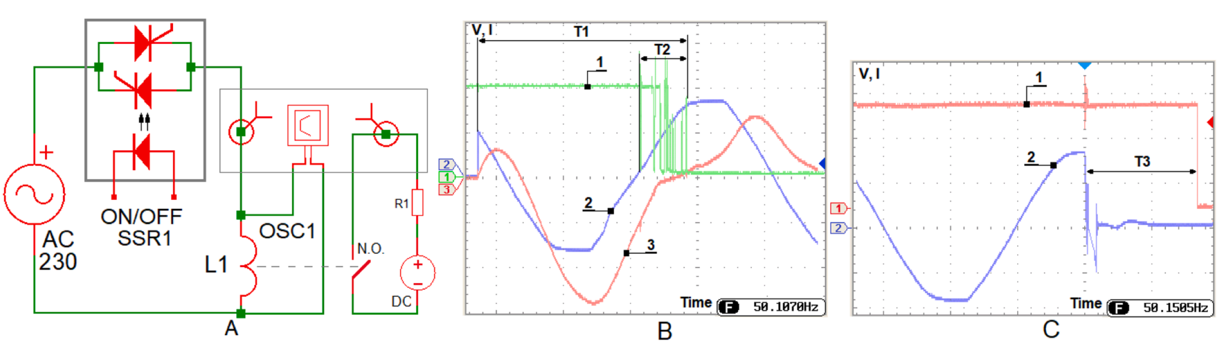

Fig. 9. Experimental verification of AC electromagnetic contactor at transient conditions, estimating the contactor turn-on and turn-off. A – Experimental circuit; B – Turn-on time (T1 = 16.35 ms), contacts vibration time (T2 = 3.41 ms), current through the contactor's contacts (1), sinusoidal voltage on the contactor's coil (2), peak voltage through the contactor's coil (3); C – Turn-off time (T3 = 8.45 ms), current through the contactor's contacts (1), and the voltage on the contactor's coil (2).

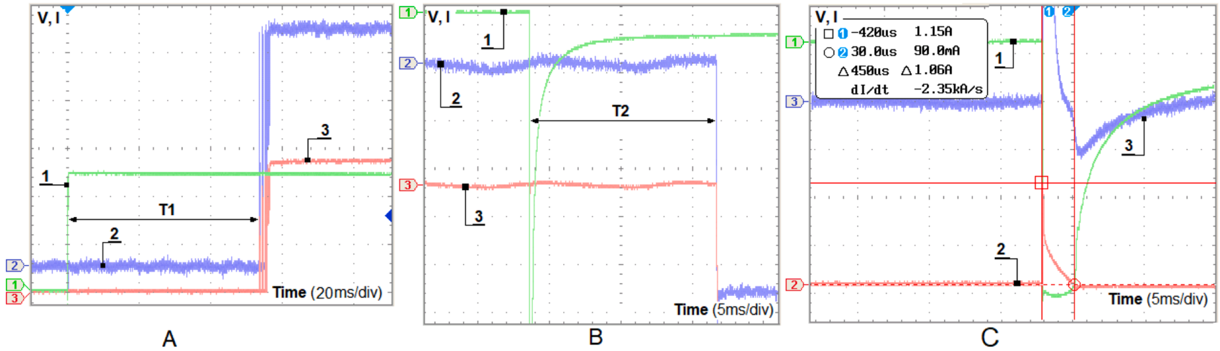

Fig. 10. Experimental verification of DC electromagnetic contactor. A – Turn-on time (T1 = 54 ms), DC voltage on the contactor coil (1), the voltage over the supplied load (2) and current (3) through the contactor's contacts; B – Turn-off time (T2 = 13.1 ms), DC voltage on the contactor coil (1), voltage (2) and current (3) through the contactor's contacts; C – voltage peak limitation of the VDR1 (Fig. 3), DC voltage on the contactor coil (1), current through the VDR (2) and current (3) through the contactor's contacts.

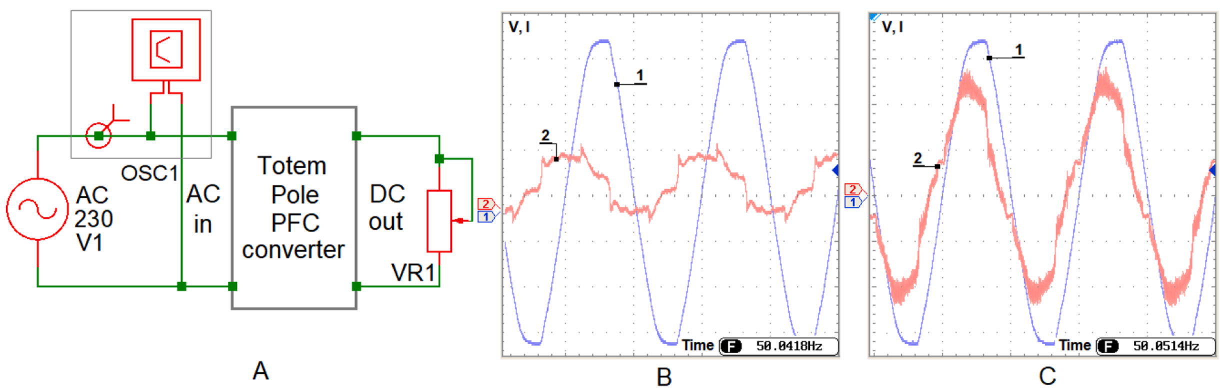

Fig. 11. Experimental verification of Totem-Pole PFC converter. A – experimental circuit; B – input voltage (1) and current (2) at stand-by conditions; C - input voltage (1) and current (2) at nominal power and PFC operation.

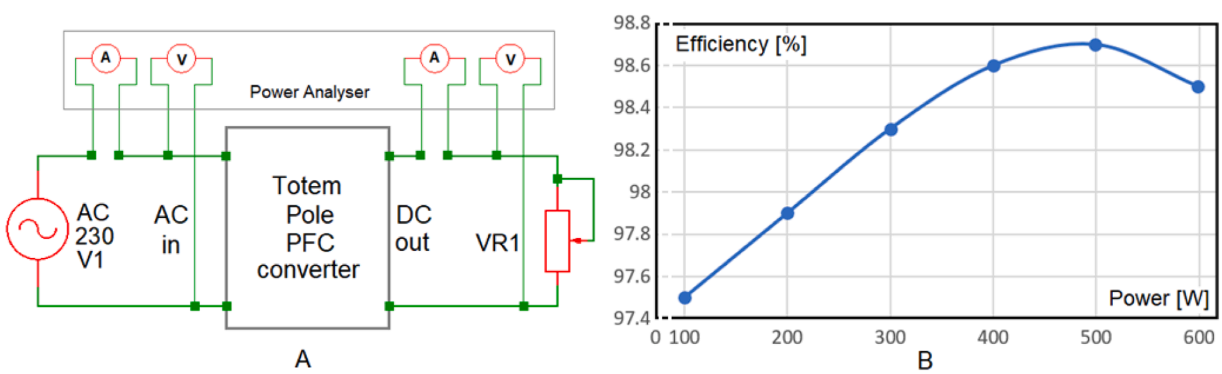

Fig. 12. Experimental verification of the efficiency of the Totem-Pole PFC converter. A – Experimental circuit; B – Efficiency vs converter power.

the contacts (1), and increase of the contactor's coil current (2) up to the peak current as shown in Fig. 8C, waveform 2. The exact process is depicted in better resolution in Fig. 14B.

The control of the DC electromagnetic contactor with the output full-bridge circuit is experimentally tested according to Fig. 15A. The permanent ON impulse (1) is supplied to transistors Q6 and Q9, and the supply in the reverse connection during the turn-off time is supplied by a single impulse (2) with duration T1 = 7.5 ms on transistors Q8 and Q7. The turn-off time is reduced to T2 = 9.6 ms registered with the contacts current (3). The voltage over the contactor's coil is limited to double the supplied voltage in the opposite direction (4).

An alternative version of the power supply system is presented in Fig. 16A.

The modification shown in Fig. 16 reduces the contractor's turn-on time. In this circuit, the Totem-Pole PFC converter and the Buck converter are not changed, as the primary amendment applies only to Module 3. Instead of the Full-bridge schematic, this module consists of only two switches – Q6 supplying high voltage (350V-400 V, Table 2) from the Totem-Pole and Q7 supplying the nominal voltage from the Buck converter. The switching process between Q6 and Q7 is ensured with a dead time of 150–200 ns to prevent their simultaneous operation. Diodes D3 and D4 (Fig. 16A) are added to avoid the transistors Q6 and Q7 reverse diodes conduction. The experimental circuit is given in Fig. 16B, and the obtained results in Fig. 16C. The high voltage is supplied to the contactors coil L3 during the transient turn-on process with a short impulse (1, T1 = 25 ms), which causes a time reduction of T2 = 22

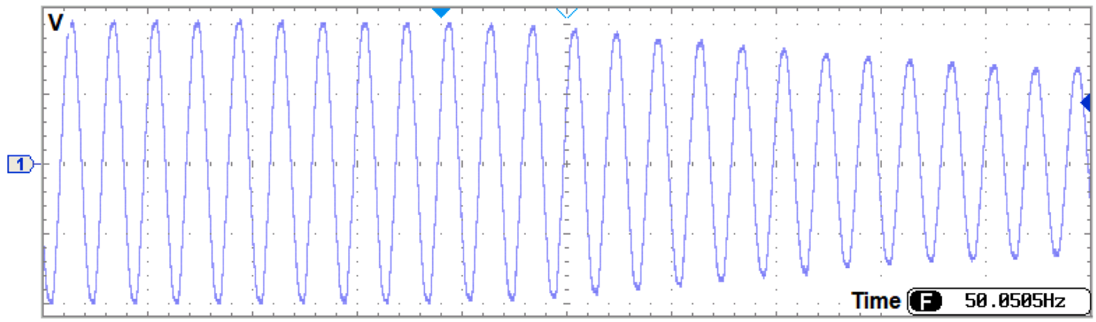

Fig. 13. Voltage sag of the power line.

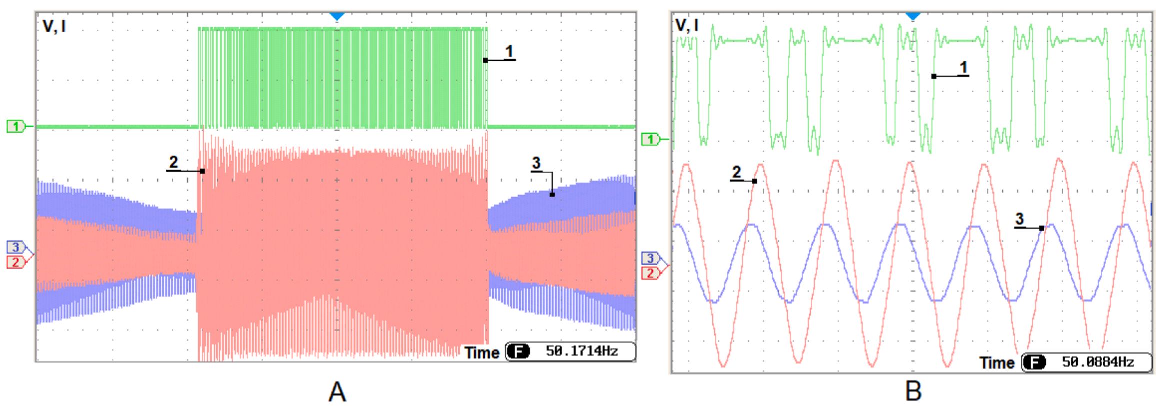

Fig. 14. AC electromagnetic contactor operation under voltage sag. A – contacts tripping under voltage sag during the entire voltage sag appearance, voltage over the contacts (1), the current through the contactor's coil (2), and the voltage over the contactor's coil (3). B – contacts tripping in a fraction of the voltage sag time, the voltage over the contacts (1), the current through the contactor's coil (2), and the voltage over the contactor's coil (3).

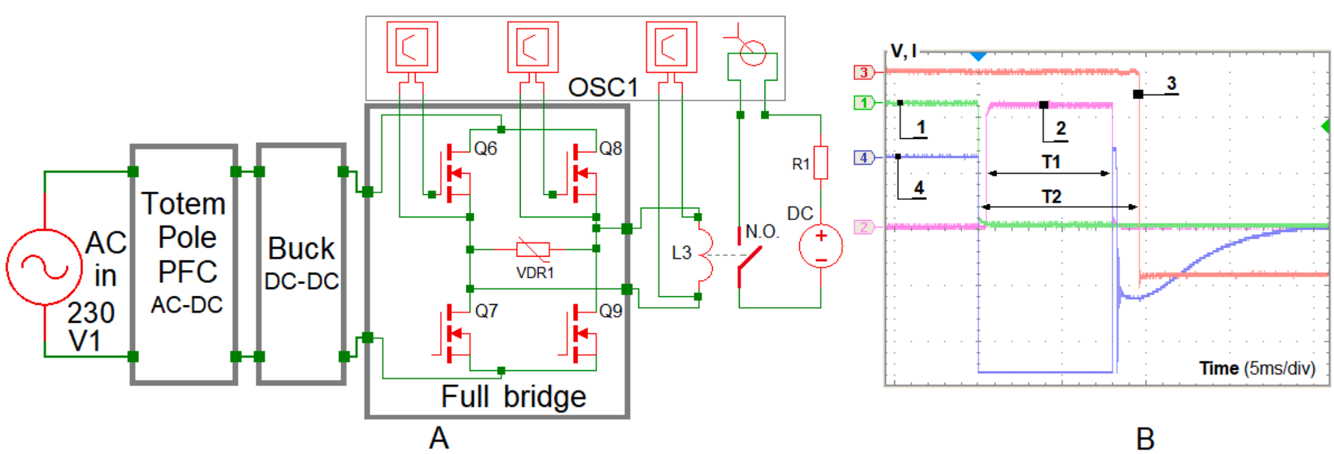

Fig. 15. Contractors control with the Full-Bridge (Fig. 3, Module 3). A – experimental verification circuit; B – turn-off transient process, PWM permanent on impulse (1), PWM reverse direction turn-off impulse (2) with duration T1 = 7.5 ms, current through the contactor's contacts (3), showing the turn-off duration of T2 = 9.6 ms, the voltage over the contactor's coil (4).

ms according to the current through the N.O. contact (2). After the turn-on process is completed, the contactor remains in a permanent ON state, supported by the transistor Q7 (4). Waveform 3 shows the voltage over the contactor coil during the entire process.

Fig. 17 offers finer details of the turn-on process of the electromagnetic contactor, which was realised in the experiments described above. The turn-on time is T1=22 ms, corresponding with the result in Fig. 16C, measured between the coil's voltage rise (3) and the contact's current (1). The current through the contacts coil is waveform 2. The experiment was conducted with high voltage and continued at 500 ms, showing no increase in the contactor's coil thermal loss during this period.

5. Conclusions

This paper offers a solution to an industrial-applied problem manifested as electromagnetic contactors malfunctioning during voltage sag. In addition, the suggested system (Fig. 2, Fig. 3) operates with PFC and is highly efficient, matching the current standards and requirements for efficiency, reliability, and compatibility.

The results from the conducted practical design and experimental

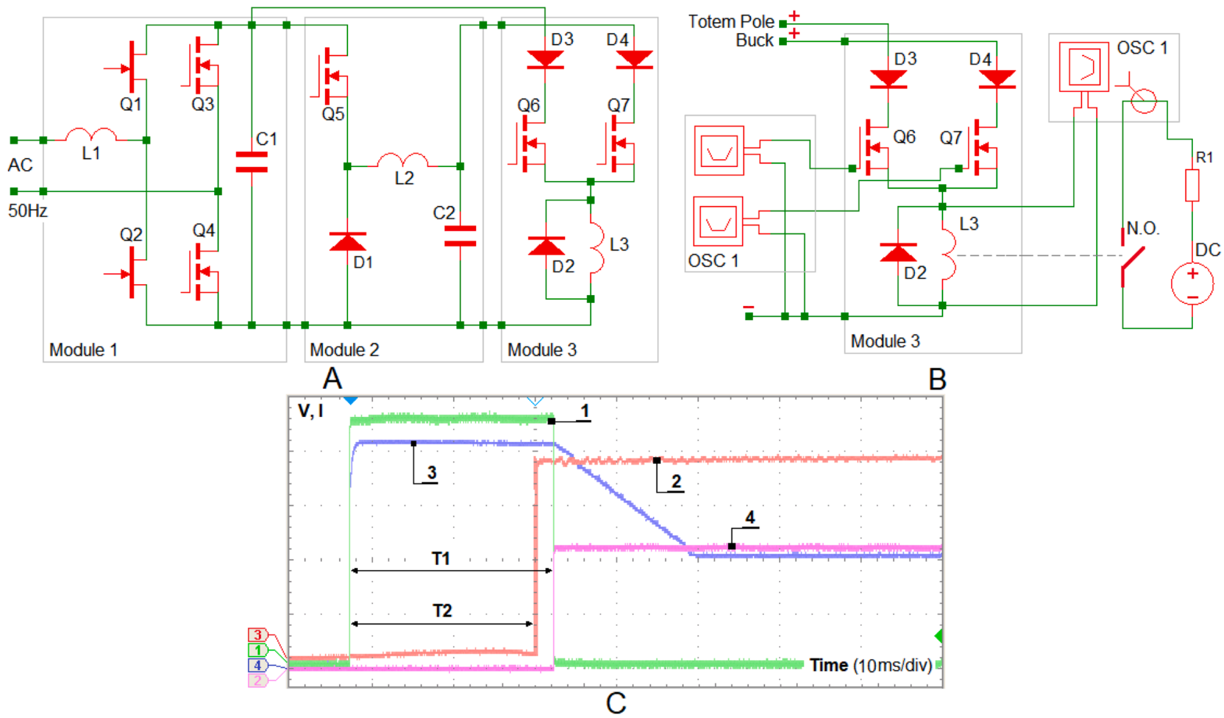

Fig. 16. An alternative version of the proposed system. A – experimental verification circuit; B – turn-on transient process, PWM turn-on impulse on transistor Q6 with duration T1 = 25 ms (1), current through the contactor's contacts (2), duration of the turn-on process T2 = 22 ms, voltage on the contactor's coil (3), PWM permanent on impulse on transistor Q7 (4).

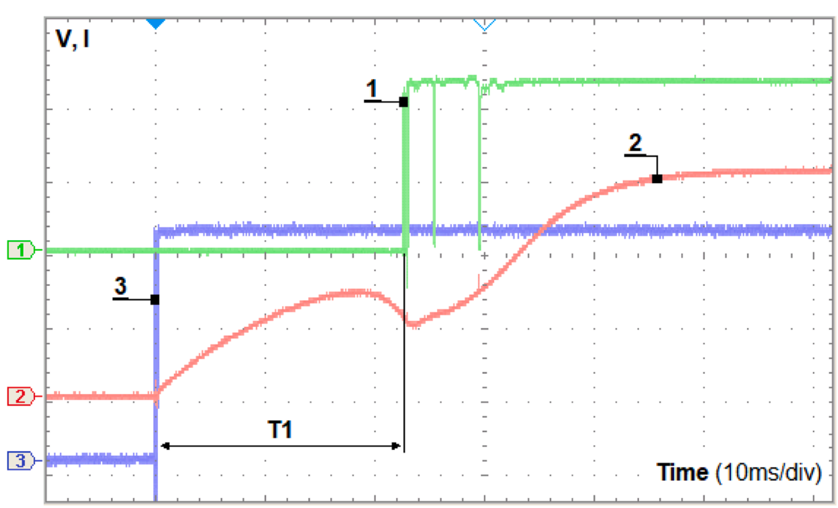

Fig. 17. Transient turn-on process of the contactor. T1 = 22 ms, current through the contactor's contacts (1), current through the contactor's coil (2), and voltage on the contactor's coil (3).

verification of the suggested power supply for electromagnetic systems of AC and DC contactors can be summarised as follows:

- The voltage sag (Fig. 13) has a detrimental effect on the electromagnetic contactors, causing contact tripping and an unacceptable increase in the coil's current. This can damage the contactor or the appliances supplied by it.
- The Totem-pole PFC converter is applicable for the suggested topology, operating stably during the voltage sag at the designed output nominal power, reaching a power factor compensation of 0.98 (Fig. 11) and an efficiency of 97% (Fig. 12).
- The turn-off process with reverse voltage supported by the H-Bridge contributes to the time reduction and overvoltage limitation (Fig. 15). This approach can be recommended for critical applications of safety systems, where minimising the turn-off time is of primary importance.
- The turn-on time could also be reduced with the circuit in Fig. 16, which switches between high and nominal voltages. The time reduction in the experimentally verified system is from 54 ms to 22 ms. The high-voltage control impulse duration could be considered equal to the expected turn-on time, which does not increase the electromagnetic system power loss.
- The design procedure (Table 2 and Table 3) for the three modules (Fig. 3) gives correct results, which have been experimentally verified and can be recommended for future research and development.

CRediT authorship contribution statement

Borislav Dimitrov: Writing – review & editing, Writing – original draft, Visualization, Validation, Methodology, Investigation, Conceptualization. **Khaled Hayatleh:** Writing – review & editing, Methodology, Formal analysis. **Sylvia Konaklieva:** Writing – review & editing, Resources, Formal analysis.

Declaration of competing interest

The authors declare that they have no known competing financial interests or personal relationships that could have appeared to influence the work reported in this paper.

Data availability

No data was used for the research described in the article.

Appendix

Table A.1
PFC Totem-pole (Module 1, Fig. 2) main design equations.

PFC Totem-Pole power part Desing	
Inductor inductance (L) and maximum current (I_{Lmax})	
$L_1 = \frac{V^2_{ACmax}}{V_{r\%} \times P_{out}} \left(1 - \frac{\sqrt{2} \times V_{ACmax}}{V_{out}}\right) \times T$ (1) $I_{Lmax} = \frac{\sqrt{2} \times P_{out}}{V_{ACmax}} \left(1 + \frac{V_{r\%}}{2}\right)$ (2) $I_{Lrms} = \frac{P_o}{V_{ACmax}}$ (3) $P_{Lcond} = I^2_{Lrms} \times R_{DC}$ (4) $P_{L.total} = P_{Lcond} + P_{Lcore}$ (5) Where: L_1 is the inductance of the input inductor; V_{ACmax} is the maximum input AC voltage; $V_{r\%}$ is the voltage ripples in percentage; P_{out} – nominal output power; V_{out} is the output voltage; T is the period ($T = 1/F_{sw}$); I_{Lmax} is the maximum inductor current; I_{Lrms} is the inductor RMS current; P_{Lcond}, P_{Lcore}, $P_{L.total}$ are respectively the conducting, core and total power losses (software estimated in this research); R_{DC} is the inductor resistance.	
High-Frequency Side Q1, Q2	Low-Frequency Side Q3, Q4
$I_{sw} = \frac{P_o}{V_{ACmax}} \times \sqrt{1 - \frac{8\sqrt{2} \times V_{ACmax}}{3\pi V_{out}}}$ (6) $P_{cond.sw} = I^2_{Boost.sw} \times R_{ON}$ (7) $I_{Lavg} = \frac{P_o}{V_{ACmax}} \times \frac{2\sqrt{2}}{\pi}$ (8) $P_{switch.sw} = (E_{on} + E_{off}) \times F_{sw}$ (9) $P_{Total.sw} = P_{cond.sw} + P_{switch.sw}$ (10) $I_{Boost.R} = \frac{P_o}{V_{ACmax}} \times \sqrt{\frac{8\sqrt{2} \times V_{ACmax}}{3\pi V_{out}}}$ (11) $P_{cond.R} = I^2_{Boost.R} \times R_{ON}$ (12) $P_{HF.Total} = \frac{P_{Total.sw} + P_{cond.R}}{2}$ (13)	$I_{MOSFET} = \frac{P_o}{V_{ACmax}} \times \sqrt{0.5}$ (14) $P_{MOSFET.R} = I^2_{MOSFET} \times R_{ON}$ (15) Were, I_{MOSFET} is the RMS current; $P_{MOSFET.R}$ is the conducting loss.
Where, for the boost switch I_{sw} is the RMS current; $P_{cond.sw}$ is the conductive loss; R_{ON} is the transistor Drain-to-Source resistance; I_{Lavg} is the average inductor current; $P_{switch.sw}$ is the switching loss; $P_{Total.sw}$ is the total loss. For the rectifier switch: $I_{Boost.R}$ is the RMS current; $P_{cond.R}$ is the conducting loss; $P_{HF.Total}$ is the total average loss.	
Output Capacitor	
$C_1 \geq \frac{2 \times P_o \times t_{hold}}{V^2_o - V^2_{out.min}}$ (16) $R_{ESR} = \frac{\tan\delta}{2\pi f \times C_1}$ (17) $I_{C1.rms} = \sqrt{\frac{8\sqrt{2} \times P^2_o}{3\pi \times V_{ACmax} \times V_{out}} - \frac{P^2_o}{V^2_o}}$ (18) $P_{C1} = I^2_{C1.rms} \times R_{ESR}$ (19) Where: C_0 is the output capacitor; R_{ESR} is the required maximum Equivalent Series Resistance (ESR); $I_{C.rms}$ is the output capacitor RMS current; t_{hold} is the hold time; P_{C1} is the capacitor power loss.	

Table A.2
Buck converter (Module 2, Fig. 2) and Full-bridge (Module 3, Fig. 2, Fig. 3) design equations.

Buck DC-DC power part Design
$D_{max} = \frac{V_{out}}{V_{in.min}}$; $D_{min} = \frac{V_{out}}{V_{in.max}}$ (20) $L_2 = \frac{V_{out}}{F_{sw}} \times \frac{1 - D}{\Delta I_{L1}}$ (21) $I_{pk} = I_{out} + \frac{\Delta I_L}{2}$ (22)

(continued on next page)

Table A.2 (*continued*)

Buck DC-DC power part Design
$P_{DCRloss.buck} = I_{out}^2 \times R_{DCon}$ (23) $P_{ON} = \frac{V_{IN} \times I_{out}}{2} \times t_{ON} \times F_{SW}$; $P_{OFF} = \frac{V_{IN} \times I_{out}}{2} \times t_{OFF} \times F_{SW}$ (24) $P_{SW} = P_{ON} + P_{OFF}$ (25) $P_{Total} = P_{SW} + P_{DCRloss}$ (26) $P_{VFD1} = V_{FD1} \times I_{out} \times (1 - D_{min})$ (27) $P_{swD1} = Q_{rr} \times V_{in} \times F_{sw}$ (28) $P_{D1total} = P_{swD1} + P_{VFD1}$ (29) $C_{out\ (min)} \geq \frac{\Delta I_{L1}}{8 \times F_{SW} \times \Delta V_{out}}$; $C_{in} \geq \frac{I_{out}}{F_{sw} \times V_{in\ pp}} \times [D \times (1 - D)]$ (30) Where: L_2 is the inductance of the Buck inductor; D_{max} *and* D_{min} are the maximum and minimum duty cycles; $V_{in.max}$ and $V_{in.min}$ are the maximum and minimum input voltages; I_{pk} is the peak current; $P_{DCRloss.buck}$ is the conducting power loss; P_{SW} is the switching current calculated from ON-time P_{ON} and OFF-time P_{OFF} loss; P_{Total} is the total transistor loss; P_{VFD1} is diode conducting loss; P_{swD1} is the dode switching loss; $P_{D1total}$ is the diode total loss; $C_{out\ (min)}$ and C_{in} are the output and input capacitors.
H-Bridge power part (Q6-Q9) design equations
$P_{MOSFET.H.bridge} = I_{L2}^2 \times R_{DCon}$ (31) $P_{DCRloss.H.bridge} = 2 \times P_{MOSFET.H.bridge}$ (32) Where: $P_{DCRloss.H.bridge}$ transistors conductive power loss; I_{L2} contactor electromagnetic system current; R_{DCon} transistors Drain-Source resistance.
Estimated efficiency
$\eta = \frac{P_{out}}{(P_{out} + P_{loss})} \times 100$ (33)

References

[1] ABB Catalogue, Motor protection and control AF Range contactors & overload relays 2020, (link accessed on 1/November/2022).

[2] ABB Catalogue, Motor protection and control 2022, (link accessed on 1/November/2022).

[3] Eaton catalogue, Contactors and Starters 2021, (link accessed on 1/November/2022).

[4] Siemens catalogue, Switching Devices – Contactors and Contactor Assemblies – for Switching Motors 2020, (link accessed on 1/November/2022).

[5] S. Dong, Driving High-Voltage Contactors in EV and HEVs. Texas Instruments Technical White Paper, SLVAF, 2021, p. 35.

[6] G. Wang, Y. Wang, L. Zhang, S. Xue, E. Dong, J. Zou, A Novel Model of Electromechanical Contactors for Predicting Dynamic Characteristics, Energies. (Basel) 14 (2021) 7466, https://doi.org/10.3390/en14227466.

[7] Y. Qiao, G. Zhai, D. Ding, X. Du, H. Zhang, C. Zhou, Robust design of dynamic characteristics consistency of Busbar-Mounted Electromagnetic Contactor based on a fast calculation surrogate model, in: 2022 IEEE 67th Holm Conference on Electrical Contacts (HLM), Tampa, FL, USA, 2022, pp. 1–7, https://doi.org/10.1109/HLM54538.2022.9969771.

[8] N. Gabdullin, J.-S. Ro, Analysis of nonlinear dynamics of permanent magnet magnetic contactor via novel computationally efficient analytical method considering stray and leakage fluxes, IEEe Access. 8 (2020) 57273–57282, https://doi.org/10.1109/ACCESS.2020.2982462.

[9] J.-W. Kang, H.-K. Jung, J.-S. Ro, H.-S. Kwon, Design of an AC magnetic contactor with a permanent magnet, in: 2018 21st International Conference on Electrical Machines and Systems (ICEMS), 2018, pp. 2826–2828, https://doi.org/10.23919/ICEMS.2018.8549029.

[10] I.C. Popa, A. Dolan, Numerical model for a plunger-type AC electromagnet, in: 2017 International Conference on Electromechanical and Power Systems (SIELMEN), Iasi, Romania, 2017, pp. 078–081, https://doi.org/10.1109/SIELMEN.2017.8123309.

[11] A. Dolan, Improvement of static force characteristic of AC electromagnet using DOE and FEM, in: 2018 International Conference on Applied and Theoretical Electricity (ICATE), Craiova, Romania, 2018, pp. 1–5, https://doi.org/10.1109/ICATE.2018.8551373.

[12] Ž.V. Despotović, B. Čupić, Đ. Lekić, Design and verification of 22kW /220Vdc electromagnet for separation of steel parts from coal on conveyor belts for delivery, in: 2022 21st International Symposium INFOTEH-JAHORINA (INFOTEH), East Sarajevo, Bosnia and Herzegovina, 2022, pp. 1–6, https://doi.org/10.1109/INFOTEH53737.2022.9751300.

[13] S. Sun, J. Cui, T. Du, Research on the influence of vibrations on the dynamic characteristics of AC contactors based on energy analysis, Energies. (Basel) 13 (3) (2020) 559, https://doi.org/10.3390/en13030559.

[14] Z. Wu, G. Wu, C. Chen, Y. Fang, L. Pan, H. Huang, A novel breaking strategy for electrical endurance extension of electromagnetic alternating current contactors, IEEE Trans. Comp., Packag. Manuf. Technol. 6 (5) (2016) 749–756, https://doi.org/10.1109/TCPMT.2016.2542101. May.

[15] C. Yang, Z. Zheng, W. Ren, Investigation of making process and associated contact bounce behaviors for alternating current contactor, in: 2021 IEEE 66th Holm Conference on Electrical Contacts (HLM), San Antonio, TX, USA, 2021, pp. 165–170, https://doi.org/10.1109/HLM51431.2021.9671183.

[16] S. Xia, et al., Research And Design Of AC Contactor For Aircraft, in: 2020 29th International Symposium on Discharges and Electrical Insulation in Vacuum (ISDEIV), Padova, Italy, 2021, pp. 375–379, https://doi.org/10.1109/ISDEIV46977.2021.9587176.

[17] X. Juna, H. Junjia, Z. Chunyan, Dynamic Analysis of Contact Bounce of Aerospace Relay Based on Finite Difference Method, Chinese J. Aeronautics 22 (2009) 262–267.

[18] C. Hung, Contact-Bounce Control and Remote Monitoring Interface Implementation of a PM Contactor, Wseas Trans. Syst. Control 6 (5) (2011). May.

[19] P. Moraes, A. Perin, An Electronic Control Unit for Reducing Contact Bounce in Electromagnetic Contactors, IEEE Trans. Industrial Electronics 55 (2) (2008).

[20] E. Ramirez-Laboreo, C. Sagues, S. Llorente, A New Run-to-Run Approach for Reducing Contact Bounce in Electromagnetic Switches, IEEE Trans. Industrial Electronics 64 (1) (2017) 535–543, https://doi.org/10.1109/TIE.2016.2605622. Jan.

[21] S. Sravanthi, R. Dheenadhayalan, M.P. Sakthivel, K. Devan, K. Madhusoodanan, A Method for Online Diagnostics of Electromagnetic Relays Against Contact Welding for Safety Critical Applications, IEEE Trans. Components, Packaging Manuf. Technol. 5 (12) (Dec. 2015) 1734–1739, https://doi.org/10.1109/TCPMT.2015.2498624.

[22] Y. Zhang, Z. Zheng, W. Ren, Y. Zhang, Investigation on switching capability of bridge structures within power electromagnetic relays, in: 2022 IEEE 67th Holm Conference on Electrical Contacts (HLM), Tampa, FL, USA, 2022, pp. 1–7, https://doi.org/10.1109/HLM54538.2022.9969837.

[23] D. Smugala, M. Bonk, Switching Arc Energy Limitation Approach for LV Circuit Breakers, Energies. (Basel) 14 (2021) 6774, https://doi.org/10.3390/en14206774.

[24] D. Shin, Y. Lee, J. Oh, Study of Arc Motion and Switching Performance in DC Magnetic Contactors, in: 2022 6th International Conference on Electric Power Equipment - Switching Technology (ICEPE-ST), Seoul, Korea, Republic of, 2022, pp. 153–156, https://doi.org/10.1109/ICEPE-ST51904.2022.9757086.

[25] M. Buffo, J.-P. Martin, S. Saadate, J. Andrea, N. Dumoulin, E. Guillard, Study of the electric arc in DC contactors: modeling, simulation and experimental validation, in: 2017 IEEE Holm Conference on Electrical Contacts, Denver, CO, USA, 2017, pp. 12–18, https://doi.org/10.1109/HOLM.2017.8088057.

[26] J. Yin, S. Yu, S. Ge, C.Liu X.Liu, Simulation Analysis of Arc Interruption Characteristics in Disconnector, Machines 10 (2022) 6, https://doi.org/10.3390/machines10010006.

[27] S. Fang, Y. Chen, H. Ni, H. Lin, X. Wang, B. Zhu, Y. Zhang, A Novel Breaking Strategy for Reduced Response Time of Electromagnetic Contactor by Reverse Voltage Application, Energies. (Basel) 12 (5) (2019) 789, https://doi.org/10.3390/en12050789.

[28] C. Zhang, Z. Xu, A Digital Controller for Series of AC Contactors, in: 2019 5th International Conference on Electric Power Equipment - Switching Technology (ICEPE-ST), 2019, pp. 702–705, https://doi.org/10.1109/ICEPE-ST.2019.8928750.

[29] B. Dimitrov, A. Cruden, A. Marinov, Modelling, analysis and verification of a resonant LLC converter as a power supply for the electromagnetic driving mechanism of an electromagnetic contactor, in: 2016 19th International

Symposium on Electrical Apparatus and Technologies (SIELA), 2016, pp. 1–4, https://doi.org/10.1109/SIELA.2016.7542988.
[30] J. Cheng, Z. Zhang, L. Chen, Close-Loop Current Control With Current-Sensing Resistor for Electromagnet Driven by Full-Bridge PWM Inverter, IEEe Access. 10 (2022) 71177–71185, https://doi.org/10.1109/ACCESS.2022.3188002.
[31] Y. Xu, R. Li, X. Rong, Y. Gao, X. Sui, Integrated Simulation of AC Contactor Based on Resonant Pole Inverter, in: 2021 IEEE International Conference on Electrical Engineering and Mechatronics Technology (ICEEMT), Qingdao, China, 2021, pp. 106–112, https://doi.org/10.1109/ICEEMT52412.2021.9602554.
[32] D. Smugala, J. Gebczyk, M. Wawro, W. Czuchra, Near-to-Zero Switching Synchronisation Approach for DC Electromagnet Actuated Relays, IEEE Trans. Industrial Electronics 69 (11) (2022) 11490–11498, https://doi.org/10.1109/TIE.2021.3118373. Nov.
[33] X. Gao, D. Yang, E. Cui, Z. Ma, H. Zhang, Study on uninterrupted switching topology and its control strategy of voltage sag protection, in: 2017 IEEE Industry Applications Society Annual Meeting, 2017, pp. 1–9, https://doi.org/10.1109/IAS.2017.8101890.
[34] M. Călin, E. Helerea, Aspects Regarding Testing of Electromagnetic Contactors Sensitivity to Voltage Dips, in: 2020 International Symposium on Fundamentals of Electrical Engineering (ISFEE), Bucharest, Romania, 2020, pp. 1–6, https://doi.org/10.1109/ISFEE51261.2020.9756156.
[35] L. Tang, Y. Han, P. Yang, C. Wang, A. Zalhaf, A review of voltage sag control measures and equipment in power systems, Energy Reports 8 (Supplement 10) (2022) 207–216. November.
[36] D. Yang, X. Gao, Z. Ma, E. Cui, H. Zhang, Novel Voltage Sag Protection Topology of Contactors for Uninterrupted Switching Capability, IEEe Trans. Ind. Appl. 54 (4) (2018) 3170–3178, https://doi.org/10.1109/TIA.2018.2822812. July-Aug.
[37] Y. Tao, Q. Jia, H. Dong, S. Xue, L. Sun, P. Li, Tolerance Evaluating of AC Contactors to Irregular Sags With Differential Strategy, IEEE Trans. Power Delivery 37 (3) (June 2022) 2413–2416, https://doi.org/10.1109/TPWRD.2022.3143357.
[38] K. Chen, Z. Qiu, C. Wu, C. Song, Compensation of Voltage Sags and Swells Using Dynamic Voltage Restorer Based on Bi-Directional H-Bridge AC/AC Converter, Processes 9 (2021) 1541, https://doi.org/10.3390/pr9091541.
[39] B. Dimitrov, Direct Off-Line Two-Switch Forward Converter With A Boost PFC Converter for Powering of DC Electromagnet Systems, Technology Education Management Informatics TEM J. 7 (1) (2018) 3–12, https://doi.org/10.18421/TEM71-01. ISSN 2217-8309February.
[40] R. Ortiz-Castrillón, G. Mejía-Ruíz, N. Muñoz-Galeano, J. López-Lezama, S. Saldarriaga-Zuluaga, PFC Single-Phase AC/DC Boost Converters: bridge, Semi-Bridgeless, and Bridgeless Topologies, Appl. Sci. 11 (2021) 7651, https://doi.org/10.3390/app11167651.
[41] R.S.-c. Yeung, J.W.-t. Fan, H.S.-h. Chung, A totem-pole PFC using hybrid pulse-width-modulation scheme, in: 2017 IEEE 3rd International Future Energy Electronics Conference and ECCE Asia (IFEEC 2017 - ECCE Asia), Kaohsiung, Taiwan, 2017, pp. 1286–1290, https://doi.org/10.1109/IFEEC.2017.7992229.
[42] Nguyen-Nghia Do, Bing-Siang Huang, Nhat-Truong Phan, Tan-Tung Nguyen, Jian-Hong Wu 1, Yu-Chen Liu, Huang-Jen Chiu, Design and Implementation of a Control Method for GaN-Based Totem-Pole Boost-Type PFC Rectifier in Energy Storage Systems, Energies. (Basel) 13 (2020) 6297, https://doi.org/10.3390/en13236297.
[43] B. Kwak, J. Kim, Digital Implementation Method for Synchronous PWM Control of GaN Transistor at Zero-Crossing of Totem-Pole PFC in Energy Storage Applications, Electronics. (Basel) 10 (2021) 30, https://doi.org/10.3390/electronics10010030.
[44] L. Qiqi, L. Bangyin, D. Shanxu, Simplified Analytical Model for Estimation of Switching Loss of Cascode GaN HEMTs in Totem-pole PFC Converters, Chinese J. Electrical Eng. 5 (3) (2019). September.
[45] Y.-Y. Huang, Y.-S. Lai, Novel Efficiency Optimized Inductor Design for GaN-Based Totem-Pole PFC, in: 2022 IEEE 31st International Symposium on Industrial Electronics (ISIE), Anchorage, AK, USA, 2022, pp. 933–938, https://doi.org/10.1109/ISIE51582. 2022.9831531.
[46] Infineon Technology, CoolGaN™ totem-pole PFC design guide and power loss modelling, 2019.
[47] Infineon Technology, 3300 W continuous conduction mode totem pole PFC with 600 V CoolMOS™ CFD7 and XMC™, 2021.

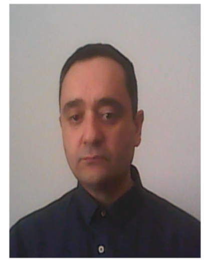

Borislav Dimitrov received his MSc and PhD from the Technical University of Varna, Bulgaria, in 2000 and 2006, respectively. His area of study is Electrical/Electronics engineering. From 1996–2006, he worked as an electrical/electronic engineer at a Thermal Power Plant, from 2006 to 2015 at the Technical University of Varna as an associate professor, 2015–2019 at the University of Southampton UK as a researcher, and from 2019 to 2021 as a senior lecturer at Oxford Brookes University, UK. Since 2021, he has worked as a lecturer and researcher at Warwick University, UK. Since 2000, he has worked on many projects in power electronics, induction heating systems, switched-mode power supplies, renewable energy generation, and their application fields. He has significant experience in the industry as a power supply designer and research & development electronics engineer gained from cooperation with several companies.

Professor Khaled Hayatleh received his BEng in 1992 from Oxford Brookes University and subsequent PhD in 1996 from Oxford Brookes University in collaboration with Imperial College, London. His research interests are in the area of electronic circuits and systems for Biomedical and High Voltage (predominantly Electric Vehicles) applications. Current projects include, the design and development of high-precision, low-power amplifiers for wearable biomedical monitors, artefact minimisation for biomedical monitoring equipment, electrical impedance tomography for breast cancer screening, driver awareness sensing system, and battery management systems for electric vehicles. He has over 100 publications in the above areas of research. He has been a keynote speaker at a number of conferences in these areas. He is currently the lead for Electronics and also Head of the Biomedical Imaging and Instrumentation Research Team at Oxford Brookes University, UK.

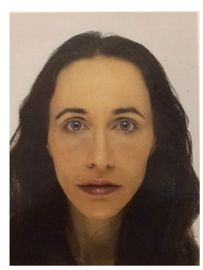

Dr Silvia Konaklieva started her engineering journey with MEng in Renewable Energy from Exeter University following which she had two years of industrial experience in the commercial solar PV sector. She moved to offshore wind research as a KTP design engineer at the Offshore Renewable Energy Catapult (formerly Narec) in Blyth, Northumberland. This role focused on developing a condition monitoring solution for power modules and converters in offshore wind turbines using electrical and thermal signatures in conjunction with artificial neural networks. Following the end of this contract her work progressed into a Power Electronics PhD at the University of Warwick's School of Engineering. After its completion she joined Professor Richard McMahon's Power Electronic and Electrical Machines and Drives research group at WMG to work on power electronic converters for battery systems and special EV charging applications. She is currently Lead Engineer coordinating the delivery of several Innovate UK and commercial subcontract projects focused on wireless charging for transport applications, including the complete design, build and EV integration (on a BMW i3) of a 20 kW wireless charging system publicly demonstrated at several general public and industry focused events at Milton Keynes currently installed and working at WMG.